Search for pair-produced heavy scalars in Z^0 decays

P. Abreu, W. Adam, T. Adye, E. Agasi, I. Azhinenko, R. Aleksan, G.D. Alekseev, P. Allport, S. Almehed, F.M.L. Almeida, et al.

EUROPEAN ORGANIZATION FOR NUCLEAR RESEARCH

CERN–PPE/94–83

6 June 1994

Search for pair-produced heavy scalars in Z^0 decays

DELPHI Collaboration

Abstract

A search for charged Higgs bosons decaying into quarks is described, based on statistics of around 1.7 million hadronic Z^0 decays detected in DELPHI. Despite the very high background from standard hadronic decays of the Z^0, masses in the range up to 43.5 GeV/c^2 are excluded at the 95% confidence level. After combination with a search for leptonic decays, this mass limit is extended to cover all branching ratios. A similar analysis sets new limits on the possible production of any pair-produced heavy scalar decaying into a pair of jets, such as neutral Higgs bosons in a two doublet scheme and diquarks.

(Submitted to Zeit. für Phys. C)

P.Abreu[20], W.Adam[7], T.Adye[37], E.Agasi[30], I.Ajinenko[42], R.Aleksan[39], G.D.Alekseev[14], P.P.Allport[21], S.Almehed[23], F.M.L.Almeida[47], S.J.Alvsvaag[4], U.Amaldi[7], A.Andreazza[27], P.Antilogus[24], W-D.Apel[15], R.J.Apsimon[37], Y.Arnoud[39], B.Åsman[44], J-E.Augustin[18], A.Augustinus[30], P.Baillon[7], P.Bambade[18], F.Barao[20], R.Barate[12], D.Y.Bardin[14], G.J.Barker[34], A.Baroncelli[40], O.Barring[7], J.A.Barrio[25], W.Bartl[50], M.J.Bates[37], M.Battaglia[13], M.Baubillier[22], K-H.Becks[52], M.Begalli[36], P.Beilliere[6], P.Beltran[9], A.C.Benvenuti[5], M.Berggren[41], D.Bertrand[2], F.Bianchi[45], M.Bigi[45], M.S.Bilenky[14], P.Billoir[22], J.Bjarne[23], D.Bloch[8], J.Blocki[51], S.Blyth[34], V.Bocci[38], P.N.Bogolubov[14], T.Bolognese[39], M.Bonesini[27], W.Bonivento[27], P.S.L.Booth[21], G.Borisov[42], C.Bosio[40], B.Bostjancic[43], S.Bosworth[34], O.Botner[48], B.Bouquet[18], C.Bourdarios[18], T.J.V.Bowcock[21], M.Bozzo[11], S.Braibant[2], P.Branchini[40], K.D.Brand[35], R.A.Brenner[13], H.Briand[22], C.Bricman[2], L.Brillault[22], R.C.A.Brown[7], P.Bruckman[16], J-M.Brunet[6], L.Bugge[32], T.Buran[32], A.Buys[7], J.A.M.A.Buytaert[7], M.Caccia[27], M.Calvi[27], A.J.Camacho Rozas[41], R.Campion[21], T.Camporesi[7], V.Canale[38], K.Cankocak[44], F.Cao[2], F.Carena[7], P.Carrilho[47], L.Carroll[21], R.Cases[49], C.Caso[11], E.Castelli[46], M.V.Castillo Gimenez[49], A.Cattai[7], F.R.Cavallo[5], L.Cerrito[38], V.Chabaud[7], A.Chan[1], M.Chapkin[42], Ph.Charpentier[7], J.Chauveau[22], P.Checchia[35], G.A.Chelkov[14], L.Chevalier[39], P.Chliapnikov[42], V.Chorowicz[22], J.T.M.Chrin[49], V.Cindro[43], P.Collins[34], J.L.Contreras[18], R.Contri[11], E.Cortina[49], G.Cosme[18], G.Cosmo[46], F.Couchot[18], H.B.Crawley[1], D.Crennell[37], G.Crosetti[11], J.Cuevas Maestro[33], S.Czellar[13], E.Dahl-Jensen[28], J.Dahm[52], B.Dalmagne[18], M.Dam[32], G.Damgaard[28], E.Daubie[2], A.Daum[15], P.D.Dauncey[37], M.Davenport[7], J.Davies[21], W.Da Silva[22], C.Defoix[6], P.Delpierre[26], N.Demaria[34], A.De Angelis[7], H.De Boeck[2], W.De Boer[15], S.De Brabandere[2], C.De Clercq[2], M.D.M.De Fez Laso[49], C.De La Vaissiere[22], B.De Lotto[46], A.De Min[27], L.De Paula[47], H.Dijkstra[7], L.Di Ciaccio[38], F.Djama[8], J.Dolbeau[6], M.Donszelmann[7], K.Doroba[51], M.Dracos[8], J.Drees[52], M.Dris[31], Y.Dufour[7], F.Dupont[12], D.Edsall[1], R.Ehret[15], T.Ekelof[48], G.Ekspong[44], M.Elsing[52], J-P.Engel[8], N.Ershaidat[22], M.Espirito Santo[20], V.Falaleev[42], D.Fassouliotis[31], M.Feindt[7], A.Fenyuk[42], A.Ferrer[49], T.A.Filippas[31], A.Firestone[1], H.Foeth[7], E.Fokitis[31], F.Fontanelli[11], F.Formenti[7], J-L.Fousset[26], S.Francon[24], B.Franek[37], P.Frenkiel[6], D.C.Fries[15], A.G.Frodesen[4], R.Fruhwirth[50], F.Fulda-Quenzer[18], H.Furstenau[7], J.Fuster[7], D.Gamba[45], M.Gandelman[17], C.Garcia[49], J.Garcia[41], C.Gaspar[7], U.Gasparini[35], Ph.Gavillet[7], E.N.Gazis[31], D.Gele[8], J-P.Gerber[8], P.Giacomelli[7], D.Gillespie[7], R.Gokieli[51], B.Golob[43], V.M.Golovatyuk[14], J.J.Gomez Y Cadenas[7], G.Gopal[37], L.Gorn[1], M.Gorski[51], V.Gracco[11], F.Grard[2], E.Graziani[40], G.Grosdidier[18], P.Gunnarsson[44], J.Guy[37], U.Haedinger[15], F.Hahn[52], M.Hahn[44], S.Hahn[52], S.Haider[30], Z.Hajduk[16], A.Hakansson[23], A.Hallgren[48], K.Hamacher[52], G.Hamel De Monchenault[39], W.Hao[30], F.J.Harris[34], V.Hedberg[23], R.Henriques[20], J.J.Hernandez[49], J.A.Hernando[49], P.Herquet[2], H.Herr[7], T.L.Hessing[21], E.Higon[49], H.J.Hilke[7], T.S.Hill[1], S-O.Holmgren[44], P.J.Holt[34], D.Holthuizen[30], P.F.Honore[6], M.Houlden[21], J.Hrubec[50], K.Huet[2], K.Hultqvist[44], P.Ioannou[3], P-S.Iversen[4], J.N.Jackson[21], R.Jacobsson[44], P.Jalocha[16], G.Jarlskog[23], P.Jarry[39], B.Jean-Marie[18], E.K.Johansson[44], M.Jonker[7], L.Jonsson[23], P.Juillot[8], M.Kaiser[15], G.Kalmus[37], F.Kapusta[22], M.Karlsson[44], E.Karvelas[9], S.Katsanevas[3], E.C.Katsoufis[31], R.Keranen[7], B.A.Khomenko[14], N.N.Khovanski[14], B.King[21], N.J.Kjaer[28], H.Klein[7], A.Klovning[4], P.Kluit[30], A.Koch-Mehrin[52], J.H.Koehne[15], B.Koene[30], P.Kokkinias[9], M.Koratzinos[32], A.V.Korytov[14], V.Kostioukhine[42], C.Kourkoumelis[3], O.Kouznetsov[14], P.H.Kramer[52], M.Krammer[50], C.Kreuter[15], J.Krolikowski[51], I.Kronkvist[23], W.Krupinski[16], W.Kucewicz[16], K.Kulka[48], K.Kurvinen[13], C.Lacasta[49], C.Lambropoulos[9], J.W.Lamsa[1], L.Lanceri[46], P.Langefeld[52], V.Lapin[42], I.Last[21], J-P.Laugier[39], R.Lauhakangas[13], G.Leder[50], F.Ledroit[12], R.Leitner[29], Y.Lemoigne[39], J.Lemonne[2], G.Lenzen[52], V.Lepeltier[18], T.Lesiak[35], J.M.Levy[8], E.Lieb[52], D.Liko[50], R.Lindner[52], A.Lipniacka[18], I.Lippi[35], B.Loerstad[23], M.Lokajicek[10], J.G.Loken[34], A.Lopez-Fernandez[7], M.A.Lopez Aguera[41], M.Los[30], D.Loukas[9], J.J.Lozano[49], P.Lutz[6], L.Lyons[34], G.Maehlum[15], J.Maillard[6], A.Maio[20], A.Maltezos[9], F.Mandl[50], J.Marco[41], B.Marechal[47], M.Margoni[35], J-C.Marin[7], C.Mariotti[40], A.Markou[9], T.Maron[52], S.Marti[49], C.Martinez-Rivero[41], F.Martinez-Vidal[49], F.Matorras[41], C.Matteuzzi[27], G.Matthiae[38], M.Mazzucato[35], M.Mc Cubbin[21], R.Mc Kay[1], R.Mc Nulty[21], J.Medbo[48], C.Meroni[27], W.T.Meyer[1], M.Michelotto[35], E.Migliore[45], I.Mikulec[50], L.Mirabito[24], W.A.Mitaroff[50], G.V.Mitselmakher[14], U.Mjoernmark[23], T.Moa[44], R.Moeller[28], K.Moenig[7], M.R.Monge[11], P.Morettini[11], H.Mueller[15], W.J.Murray[37], B.Muryn[16], G.Myatt[34], F.Naraghi[12], F.L.Navarria[5], P.Negri[27], S.Nemecek[10], W.Neumann[52], N.Neumeister[50], R.Nicolaidou[3], B.S.Nielsen[28], P.E.S.Nilsen[4], P.Niss[44], A.Nomerotski[35], A.Normand[34], M.Novak[10], V.Obraztsov[42], A.G.Olshevski[14], R.Orava[13], K.Osterberg[13], A.Ouraou[39], P.Paganini[18], M.Paganoni[27], R.Pain[22], H.Palka[16], Th.D.Papadopoulou[31], L.Pape[7], F.Parodi[11], A.Passeri[40], M.Pegoraro[35], J.Pennanen[13], L.Peralta[20], M.Pernicka[50], A.Perrotta[5], C.Petridou[46], A.Petrolini[11], H.T.Phillips[37], G.Piana[11], F.Pierre[39], M.Pimenta[20], S.Plaszczynski[18], O.Podobrin[15], M.E.Pol[17], G.Polok[16], P.Poropat[46], V.Pozdniakov[14], P.Privitera[38], A.Pullia[27], D.Radojicic[34], S.Ragazzi[27], H.Rahmani[31], P.N.Ratoff[19], A.L.Read[32], M.Reale[52], P.Rebecchi[18], N.G.Redaelli[27], M.Regler[50], D.Reid[7], P.B.Renton[34], L.K.Resvanis[3], F.Richard[18], J.Richardson[21], J.Ridky[10], G.Rinaudo[45], A.Romero[45], I.Roncagliolo[11], P.Ronchese[35], L.Roos[12], E.I.Rosenberg[1], E.Rosso[7], P.Roudeau[18], T.Rovelli[5], W.Ruckstuhl[30], V.Ruhlmann-Kleider[39], A.Ruiz[41], H.Saarikko[13], Y.Sacquin[39], G.Sajot[12], J.Salt[49], J.Sanchez[25], M.Sannino[11], S.Schael[7], H.Schneider[15], M.A.E.Schyns[52], G.Sciolla[45],

F.Scuri[46], A.M.Segar[34], A.Seitz[15], R.Sekulin[37], M.Sessa[46], R.Seufert[15], R.C.Shellard[36], I.Siccama[30], P.Siegrist[39], S.Simonetti[11], F.Simonetto[35], A.N.Sisakian[14], T.B.Skaali[32], G.Smadja[24], N.Smirnov[42], O.Smirnova[14], G.R.Smith[37], R.Sosnowski[51], D.Souza-Santos[36], T.Spassov[20], E.Spiriti[40], S.Squarcia[11], H.Staeck[52], C.Stanescu[40], S.Stapnes[32], I.Stavitski[35], G.Stavropoulos[9], K.Stepaniak[51], F.Stichelbaut[7], A.Stocchi[18], J.Strauss[50], J.Straver[7], R.Strub[8], B.Stugu[4], M.Szczekowski[51], M.Szeptycka[51], T.Tabarelli[27], O.Tchikilev[42], G.E.Theodosiou[9], Z.Thome[47], A.Tilquin[26], J.Timmermans[30], V.G.Timofeev[14], L.G.Tkatchev[14], T.Todorov[8], D.Z.Toet[30], A.Tomaradze[2], B.Tome[20], E.Torassa[45], L.Tortora[40], G.Transtromer[23], D.Treille[7], W.Trischuk[7], G.Tristram[6], C.Troncon[27], A.Tsirou[7], E.N.Tsyganov[14], M-L.Turluer[39], T.Tuuva[13], I.A.Tyapkin[22], M.Tyndel[37], S.Tzamarias[21], B.Ueberschaer[52], S.Ueberschaer[52], O.Ullaland[7], V.Uvarov[42], G.Valenti[5], E.Vallazza[7], J.A.Valls Ferrer[49], C.Vander Velde[2], G.W.Van Apeldoorn[30], P.Van Dam[30], M.Van Der Heijden[30], W.K.Van Doninck[2], J.Van Eldik[30], P.Vaz[7], G.Vegni[27], L.Ventura[35], W.Venus[37], F.Verbeure[2], M.Verlato[35], L.S.Vertogradov[14], D.Vilanova[39], P.Vincent[24], L.Vitale[46], E.Vlasov[42], A.S.Vodopyanov[14], M.Vollmer[52], M.Voutilainen[13], H.Wahlen[52], C.Walck[44], A.Wehr[52], M.Weierstall[52], P.Weilhammer[7], A.M.Wetherell[7], J.H.Wickens[2], M.Wielers[15], G.R.Wilkinson[34], W.S.C.Williams[34], M.Winter[8], M.Witek[7], G.Wormser[18], K.Woschnagg[48], K.Yip[34], O.Yushchenko[42], A.Zaitsev[42], A.Zalewska[16], P.Zalewski[51], D.Zavrtanik[43], E.Zevgolatakos[9], N.I.Zimin[14], M.Zito[39], D.Zontar[43], R.Zuberi[34], G.Zumerle[35]

[1] Ames Laboratory and Department of Physics, Iowa State University, Ames IA 50011, USA
[2] Physics Department, Univ. Instelling Antwerpen, Universiteitsplein 1, B-2610 Wilrijk, Belgium
and IIHE, ULB-VUB, Pleinlaan 2, B-1050 Brussels, Belgium
and Faculté des Sciences, Univ. de l'Etat Mons, Av. Maistriau 19, B-7000 Mons, Belgium
[3] Physics Laboratory, University of Athens, Solonos Str. 104, GR-10680 Athens, Greece
[4] Department of Physics, University of Bergen, Allégaten 55, N-5007 Bergen, Norway
[5] Dipartimento di Fisica, Università di Bologna and INFN, Via Irnerio 46, I-40126 Bologna, Italy
[6] Collège de France, Lab. de Physique Corpusculaire, IN2P3-CNRS, F-75231 Paris Cedex 05, France
[7] CERN, CH-1211 Geneva 23, Switzerland
[8] Centre de Recherche Nucléaire, IN2P3 - CNRS/ULP - BP20, F-67037 Strasbourg Cedex, France
[9] Institute of Nuclear Physics, N.C.S.R. Demokritos, P.O. Box 60228, GR-15310 Athens, Greece
[10] FZU, Inst. of Physics of the C.A.S. High Energy Physics Division, Na Slovance 2, 180 40, Praha 8, Czech Republic
[11] Dipartimento di Fisica, Università di Genova and INFN, Via Dodecaneso 33, I-16146 Genova, Italy
[12] Institut des Sciences Nucléaires, IN2P3-CNRS, Université de Grenoble 1, F-38026 Grenoble Cedex, France
[13] Research Institute for High Energy Physics, SEFT, P.O. Box 9, FIN-00014 Helsinki, Finland
[14] Joint Institute for Nuclear Research, Dubna, Head Post Office, P.O. Box 79, 101 000 Moscow, Russian Federation
[15] Institut für Experimentelle Kernphysik, Universität Karlsruhe, Postfach 6980, D-76128 Karlsruhe, Germany
[16] High Energy Physics Laboratory, Institute of Nuclear Physics, Ul. Kawiory 26a, PL-30055 Krakow 30, Poland
[17] Centro Brasileiro de Pesquisas Físicas, rua Xavier Sigaud 150, BR-22290 Rio de Janeiro, Brazil
[18] Université de Paris-Sud, Lab. de l'Accélérateur Linéaire, IN2P3-CNRS, Bat 200, F-91405 Orsay Cedex, France
[19] School of Physics and Materials, University of Lancaster, Lancaster LA1 4YB, UK
[20] LIP, IST, FCUL - Av. Elias Garcia, 14-1°, P-1000 Lisboa Codex, Portugal
[21] Department of Physics, University of Liverpool, P.O. Box 147, Liverpool L69 3BX, UK
[22] LPNHE, IN2P3-CNRS, Universités Paris VI et VII, Tour 33 (RdC), 4 place Jussieu, F-75252 Paris Cedex 05, France
[23] Department of Physics, University of Lund, Sölvegatan 14, S-22363 Lund, Sweden
[24] Université Claude Bernard de Lyon, IPNL, IN2P3-CNRS, F-69622 Villeurbanne Cedex, France
[25] Universidad Complutense, Avda. Complutense s/n, E-28040 Madrid, Spain
[26] Univ. d'Aix - Marseille II - CPP, IN2P3-CNRS, F-13288 Marseille Cedex 09, France
[27] Dipartimento di Fisica, Università di Milano and INFN, Via Celoria 16, I-20133 Milan, Italy
[28] Niels Bohr Institute, Blegdamsvej 17, DK-2100 Copenhagen 0, Denmark
[29] NC, Nuclear Centre of MFF, Charles University, Areal MFF, V Holesovickach 2, 180 00, Praha 8, Czech Republic
[30] NIKHEF-H, Postbus 41882, NL-1009 DB Amsterdam, The Netherlands
[31] National Technical University, Physics Department, Zografou Campus, GR-15773 Athens, Greece
[32] Physics Department, University of Oslo, Blindern, N-1000 Oslo 3, Norway
[33] Dpto. Fisica, Univ. Oviedo, C/P.Jimenez Casas, S/N-33006 Oviedo, Spain
[34] Department of Physics, University of Oxford, Keble Road, Oxford OX1 3RH, UK
[35] Dipartimento di Fisica, Università di Padova and INFN, Via Marzolo 8, I-35131 Padua, Italy
[36] Depto. de Fisica, Pontificia Univ. Católica, C.P. 38071 RJ-22453 Rio de Janeiro, Brazil
[37] Rutherford Appleton Laboratory, Chilton, Didcot OX11 OQX, UK
[38] Dipartimento di Fisica, Università di Roma II and INFN, Tor Vergata, I-00173 Rome, Italy
[39] Centre d'Etude de Saclay, DSM/DAPNIA, F-91191 Gif-sur-Yvette Cedex, France
[40] Istituto Superiore di Sanità, Ist. Naz. di Fisica Nucl. (INFN), Viale Regina Elena 299, I-00161 Rome, Italy
[41] C.E.A.F.M., C.S.I.C. - Univ. Cantabria, Avda. los Castros, S/N-39006 Santander, Spain, (CICYT-AEN93-0832)
[42] Inst. for High Energy Physics, Serpukov P.O. Box 35, Protvino, (Moscow Region), Russian Federation
[43] J. Stefan Institute and Department of Physics, University of Ljubljana, Jamova 39, SI-61000 Ljubljana, Slovenia
[44] Fysikum, Stockholm University, Box 6730, S-113 85 Stockholm, Sweden
[45] Dipartimento di Fisica Sperimentale, Università di Torino and INFN, Via P. Giuria 1, I-10125 Turin, Italy
[46] Dipartimento di Fisica, Università di Trieste and INFN, Via A. Valerio 2, I-34127 Trieste, Italy
and Istituto di Fisica, Università di Udine, I-33100 Udine, Italy
[47] Univ. Federal do Rio de Janeiro, C.P. 68528 Cidade Univ., Ilha do Fundão BR-21945-970 Rio de Janeiro, Brazil
[48] Department of Radiation Sciences, University of Uppsala, P.O. Box 535, S-751 21 Uppsala, Sweden
[49] IFIC, Valencia-CSIC, and D.F.A.M.N., U. de Valencia, Avda. Dr. Moliner 50, E-46100 Burjassot (Valencia), Spain
[50] Institut für Hochenergiephysik, Österr. Akad. d. Wissensch., Nikolsdorfergasse 18, A-1050 Vienna, Austria
[51] Inst. Nuclear Studies and University of Warsaw, Ul. Hoza 69, PL-00681 Warsaw, Poland
[52] Fachbereich Physik, University of Wuppertal, Postfach 100 127, D-42097 Wuppertal 1, Germany

1 Introduction

The Z^0 boson decay is an ideal environment for the direct search for new particles. Heavy scalars are predicted by different models, in particular a charged Higgs boson is present in all non-minimal Standard Models. This analysis is devoted to a search for the pair production of such particles in e^+e^- collisions at the Z^0 resonance.

The decay width of the Z^0 into a pair of charged Higgs particles in the framework of a two Higgs doublet scheme is given by [1] :

$$\Gamma(Z \to H^+H^-) = \frac{G_f m_Z^3}{6\pi\sqrt{2}}(1/2 - \sin^2\theta_W)^2(1 - 4m_H^2/s)^{3/2} \quad (1)$$

where G_f is the Fermi constant, m_H and m_Z are the masses of the $H^\pm$ and the Z^0 bosons, and θ_W is the electroweak mixing angle.

The experiments at PETRA [2] have placed a lower limit on the mass of the charged Higgs boson at about 19 GeV/c^2. The DELPHI Collaboration has already published an earlier analysis [3], which used about 12000 hadronic Z^0 decays and excluded the mass range from 18 to 29 GeV/c^2. The results presented here focus on the higher mass range and have been obtained using the complete data sample collected by DELPHI from 1991 to 1993. Results from the other LEP experiments can be found in ref. [4].

Since the branching ratios for the decay $H^+ \to f\bar{f}$ are model dependent, a complete analysis should include all possible decays. The major part of the present analysis assumes that these scalars decay purely hadronically. Thus the search for $Z^0 \to H^+H^- \to q\overline{q'}q'\overline{q}$ is performed by analyzing four-jet hadronic final states. Section 2 describes the various steps of the analysis which are independent of the Higgs boson mass, while section 3 deals with the results that can be extracted as a function of the Higgs boson mass. In section 3.2 results from analyses of purely leptonic decays are given and combined in section 3.3 with those from the four jet analysis in order to give a result independent of the branching ratios.

Since this four-jet analysis relies only on the hypotheses that the heavy objects are produced in pairs, that they are scalars and that they decay into two quarks, it is possible to infer limits on the masses of other objects having similar properties (neutral Higgs particles in a general two doublet scheme and diquarks). Section 4 is devoted to such a study.

2 Strategy

Details concerning the components of the DELPHI detector can be found in ref. [6]. This analysis relied primarily on tracks of charged particles reconstructed using the Time Projection Chamber, the Inner and Outer Detectors and the forward chambers, on neutral particles depositing electromagnetic energy in the barrel electromagnetic calorimeter or the forward electromagnetic calorimeter or hadronic energy in the hadron calorimeter.

All data collected by DELPHI during 1991, 1992 and 1993 were used. This sample corresponds to an integrated luminosity of 70.6 pb^{-1} (about 1.7 million hadronic Z^0 decays).

These data have been compared with more than 3 million $q\bar{q}$ events which were generated using the string fragmentation scheme from the JETSET Parton Shower model [5], together with $Z^0 \to H^+H^- \to c\bar{s}\bar{c}s$ events (around 1000 events at each of 6 different Higgs boson masses). It should be noted that this particular decay is expected to be by far the dominant hadronic decay of the Higgs boson. These generated events were processed through the DELPHI simulation package in order to measure the response of the detector.

The decay width given by expression (1) is relatively small and is evaluated in Table 1 for different $H^{\pm}$ masses. The expected number of events has been computed taking into account the correct weighting of the different energies of the data sample. It is clear from Table 1 (and Figure 1) that the major difficulty of the analysis is to exclude as far as possible the huge background due to standard hadronic processes, while keeping a reasonable efficiency for the signal.

m_H (GeV/c^2)	$\Gamma_{H^+H^-}/\Gamma_{had}$	number of expected evts / 1.7×10^6 had. Z^0
30	5.83×10^{-3}	10013
35	3.57×10^{-3}	6187
40	1.48×10^{-3}	2618
43	4.80×10^{-4}	889
45	4.43×10^{-5}	127

Table 1 : Branching ratio and number of expected events

2.1 The four-jet picture

After the preliminary selection of hadronic events (at least 7 charged particle tracks pointing to the vertex region and at least 2 jets), events with at least four jets were kept. Jets were defined using both charged and neutral particles. The jet-finding algorithm YCLUS [7] was used with a normalized cut parameter y_{cut} set to 0.02. This value was chosen to select events having four well separated jets, which is the usual case for the signal (especially for high mass values), and is seldom expected for the QCD background. Some 75% of the signal events were retained (rather independent of the generated masses) but only 8.5% of the data and 7.6% of the $q\bar{q}$ simulated Monte Carlo. The observed difference between data and simulation showed a discrepancy of 11% in the four-jet content, as illustrated in fig. 2a, which shows the ratio of simulation to data as a function of the number of jets after the jet-finding algorithm with $y_{cut} = 0.02$. A discrepancy of this size is within

the systematic error that can be expected from the error in α_s and the imperfect modeling of multijet final states implicit in the Parton Shower approach. Since the simulated $q\bar{q}$ sample is used in the following as the model for the background, in order to search for narrow structures in the di-jet mass spectrum, a further fine-tuning was necessary. This was achieved by using a slightly lower value of y_{cut} for the simulated samples (0.020) than for the data (0.0225). This resulted in a good agreement for the classification of hadronic events into 2, 3 and multi-jets, as shown in Figure 2b, and brought the di-jet mass spectra into closer agreement than before. The distributions of all other variables used in the analysis were checked, and were found not to be significantly affected. Figures 6a), 6b), 7b) and 7c) are examples of the results of these checks on crucial variables of the analysis.

Coming back to the selection of four jet events, an additional cut on shape variables was used to further suppress non-spherical events. Events were selected if $H_2 + H_4 < 0.6$ where H_2 and H_4 are two Fox-Wolfram moments (these even numbered moments are expected to be 1 for the ideal two-jet topology and zero for isotropic events) [8]. The result of this four-jet filter was to keep 65% of the signal while 96.5% of the data (and of the $q\bar{q}$ simulation) were rejected.

When an event has more than 4 jets, the extra jets are normally due to relatively soft gluons. In order to handle these events in the same framework as events directly reconstructed as four-jet, they were reanalyzed using a version of YCLUS with the number of jets fixed to four.

Thus far in the analysis, all candidate events had the same 4-jet structure, and the signal-to-background ratio, s/b, was $\sim 1/100$ for $H^{\pm}$ at 43 GeV/c^2.

Searching for pair production of heavy particles requires a pairing method and the computation of jet-jet masses. In order to achieve a precise mass reconstruction, a global constrained fit was performed on each event, imposing conservation of the total energy-momentum with the extra constraint that two jet-jet masses be equal.

The details of such a fit are described in ref. [9]. Among the three possible pairings, the one giving the best χ^2 was retained. Since the background mainly consists of $q\overline{q}gg$ events, this fit had a clear tendency to give a good χ^2 for a qg pairing with mass approaching the beam energy. Figure 3 shows the mass distributions obtained in fitting simulated signal events at three values of the $H^{\pm}$ mass m_H. It is clear from that figure that a wrong pairing is chosen in around 20% of the cases. The full width at half-maximum was found to decrease as the mass of the expected object approached the beam energy, from 2.4 GeV/c^2 at $m_H = 30$ GeV/c^2 to 0.8 GeV/c^2 at $m_H = 44.5$ GeV/c^2. This fit gave better resolution and better efficiency than methods based on simple energy rescaling. It should also be noted that the intrinsic width of the charged Higgs boson is predicted to be negligible when compared with these resolutions.

Cuts necessary to ensure the overall quality of the data and of the constrained fit (5 constraints) were then applied. Events satisfying the following criteria were retained :

- the relative error on the momentum of all charged particles had to be less than 100%,
- 30 GeV $< E_{tot} <$ 100 GeV where E_{tot} is the total visible energy (before fit),
- charged multiplicity ≥ 2 for each jet,
- that the fitted jet energies be positive,

- χ^2 (fit) ≤ 15 .

All these requirements constitute an overall quality cut, but 90% of the rejection is due to the χ^2 requirement.

Each event was then described by a set of 17 variables, namely :

- global shape variables (sphericity, thrust, aplanarity, oblateness, the first four Fox-Wolfram moments)
- four fitted jet energies (E_1 to E_4, sorted by increasing energy)
- a common di-jet mass M and a χ^2 for the global fit
- three angles : a polar production angle θ and two di-jet opening angles (α_1 and α_2)

The distributions of some of these variables should exhibit differences between the signal and the background consisting mainly of $q\overline{q}gg$ events. These two types of events are shown schematically in Figure 4.

Expected differences are :

- the opening angles (α) should be smaller for the background than for the signal. Consequently, the distributions of all shape variables should show strong differences, the signal being dominant in the small thrust – high sphericity region. However, the preliminary cut on $H_2 + H_4$ will weaken these differences.
- the least energetic jet is in general a gluon jet for a $q\overline{q}gg$ event. Thus its energy is on average smaller than that of the corresponding jet from H^+H^-, where the energies of the four quark jets are expected to be roughly equal.
- because of the scalar nature of the Higgs boson, the angular distribution of the H^+ with respect to the e^+ incoming direction will be proportional to $\sin^2\theta$, while for the background the usual $(1 + \cos^2\theta)$ behaviour is expected.

2.2 Discriminant variables

In a discriminant analysis between two groups, each variable has its own discriminating power, which can be expressed by the quantity :

$$\lambda_x = \frac{n_1 n_2}{(n_1 + n_2)^2} \frac{(\overline{x}_1 - \overline{x}_2)^2}{\sigma_x^2}$$

where :

- n_1 and n_2 are the respective sizes of the two groups.
- $\overline{x}$ indicates the mean value of the variable for each group.
- σ_x is the overall RMS deviation of variable x (for the sample obtained by merging both groups).

In this analysis, the highest value of λ was found to be 15 % for the three highly correlated variables E_1, E_4 and their difference. The lowest jet energy E_1 was kept as the best discriminating variable. A second group of variables had values of λ between 6 and 9 %. This group contained all shape variables, as well as E_2, E_3, and the opening angles of the di-jets. Sphericity ($\mathcal{S}$) was kept as second best discriminating variable because of its weak correlation with E_1. Among the remaining variables θ showed no correlation with $\mathcal{S}$ or E_1 while having a λ sufficiently high (4.5%) to improve the discrimination.

Figure 5 shows the distributions of these three variables for DELPHI data and for the simulations. A reasonable overall compatibility between experimental data and the $q\overline{q}$ simulation and a clear difference from the Higgs boson simulation were observed, providing a quantitative check of what was expected qualitatively in the previous section. It has been proven [10] that a single cut in a linear combination of appropriately chosen discriminating variables is always superior to a set of successive cuts in one variable at a time. The best linear combination of E_1, $\mathcal{S}$ and θ (let us call it F) was found by a Fisher linear discriminant analysis to be

$$F = 3.65 \times (E_1/E_1^{max}) + 2.0 \times \mathcal{S} + 2.8 \times (\theta/\theta^{max}) \qquad (2)$$

when the coefficients are optimized for discriminating 44.5 GeV/c^2 Higgs particles from the background. Here E_1^{max} is half the beam energy and θ^{max} is equal to $\pi/2$. It should be noted that the choice of these three variables was independent of the mass of the charged Higgs boson and that the coefficients in the linear combination were rather insensitive to that mass, at least for masses greater than 40 GeV/c^2. Figure 6 shows the distributions of this new variable for the same samples as in Figure 5, exhibiting a clear difference between the $q\overline{q}$ Monte Carlo simulation and any Higgs boson signal. Figure 6c also shows that there is no possibility to totally remove the background since in such a case, the remaining efficiency for the signal would be too low. A cut in F at a value of 4.5 was found to be a good compromise in optimizing both the efficiency for the signal and the rejection factor for the background. The shaded histograms in Figure 5 show the effect of this cut on the original variables for all samples.

This strategy was applied to the available samples, the DELPHI data on one hand, and various simulated data on the other. The effects of the previously defined cuts are described in Table 2, together with their global efficiencies. It should be noted that despite a reduction of the background by a factor 200, the signal/background ratio was still very small (of the order of 3×10^{-2} in the case of a 43 GeV/c^2 charged Higgs boson). The extraction of physical results from these samples is discussed in the next section.

	DELPHI data	MC $q\overline{q}$ (PS)	H^+H^- 40 GeV/c^2	H^+H^- 43 GeV/c^2	H^+H^- 44.5 GeV/c^2
normalized statistics	1,713,024	1,713,024	2618	889	268
4 jet filter and quality cut	51,097	51,180	1533	553	155
$F \geq 4.5$	9203 ± 96	9045 ± 69	641 ± 40	265 ± 17	90 ± 5
efficiency	0.54%	0.53%	24.5%	29.8%	33.6%

Table 2 : Selections and efficiencies

From Table 2, it is clear that the agreement between DELPHI data and $q\overline{q}$ simulation is satisfactory. In order to evaluate the systematic error on the simulation, the χ^2 cut (from the kinematical fit) was varied over the range 5 to 20, and the F cut over the range

4 to 5. A check was performed of the stability of the results : the MC/data ratio after the F cut was found to be stable between .98 and .99, so that the final results should not depend on the precise value of these cuts within the quoted ranges. From this check we estimated that the systematic error on the residual background obtained from the simulation was approximately 2%, including the error on the normalization.

3 Results

3.1 Hadronic channel : Comparison of mass spectra

The di-jet mass spectra shown in Figure 7 lead to the following observations :

- The data and the residual simulated background have a clear tendency to peak near the kinematical limit (around 44 GeV/c^2), as already mentioned in the paragraph concerning the kinematical fit.
- Both data and residual background distributions are smooth. Fourth order polynomials are sufficient to fit these distributions from 28 to 44.5 GeV/c^2 very well as shown in Figure 7a) (χ^2/ndf = 26.1/28 for data and 24.6/28 for the background).
- Data and the $q\overline{q}$ simulation agree reasonably well, after the y_{cut} fixing described in section 2.1 : indeed the ratio of the two distributions is flat and close to unity, in particular in the high mass region, as can be seen in Figure 7c.

In order to obtain a limit of sensitivity corresponding to the 95% confidence level for each possible mass, two different tests were performed : the first one was a direct comparison between observed data and expected background, while the second was an attempt to look for a possible signal without relying on the background simulation.

3.1.1 Significance of a difference

A test of the significance of the difference (Δ) between the observed number of events and the expected background in a given mass window of total width 2 GeV/c^2 was used to derive the sensitivity of the analysis. Since no narrow structure was expected in the $q\overline{q}$ background, a fourth order polynomial was fitted to the simulation results in order to reduce the statistical fluctuations due to the finite number of events used, and the 2% systematic error determined above was added quadratically to the statistical one deduced from the fit[†]. The 95% confidence level for the upper bound of the difference Δ has been computed taking into account the fact that Δ has a physical lower bound of zero. Numerical values obtained for four mass hypotheses are displayed in the first part of Table 3. In addition, the same procedure was applied for all mass hypotheses from 28 to 44 GeV/c^2 in 1 GeV steps. The limit of sensitivity, defined as the maximum signal at the 95% confidence level allowed by the observations, after correction for efficiency, was deduced, and is shown in Figure 8 as curve a.

[†]For practical reasons, two fits were performed to the simulation, both with a fourth order polynomial : the first one, from 28 to 44 GeV/c^2 was used for masses up to 43 GeV/c^2, the second one from 40 to 46 GeV/c^2 was necessary for the high mass region. Both fits gave similar results at 43 GeV/c^2.

mass hypothesis	37 GeV/c^2	40 GeV/c^2	43 GeV/c^2	44.5 GeV/c^2
First method : significance of Δ = data $-$ background In this case, the mass is the centre of a 2 GeV/c^2 window				
expected signal	376 ± 40	275 ± 27	155 ± 12	65 ± 4
signal efficiency	8.0%	10.5%	17.5%	24.2%
observed data	684 ± 26	1228 ± 35	2653 ± 51	3072 ± 55
background	584 ± 17	1138 ± 24	2737 ± 38	3148 ± 41
fitted background	$593 \pm 9 \pm 12$	$1137 \pm 12 \pm 23$	$2753 \pm 19 \pm 55$	$3143 \pm 20 \pm 63$
Δ	91 ± 30	91 ± 43	-100 ± 78	-71 ± 86
95% CL upper limit for Δ	140	162	100	130
sensitivity limit	1750	1540	570	540
Second method : fit data + $\alpha\times$ signal				
α	0.16 ± 0.06	0.00 ± 0.07	0.00 ± 0.04	not stable
95% CL upper lim. for α	0.26	0.14	0.08	not computable
sensitivity limit	1220	370	71	not computable

Table 3 : Tests to establish the sensitivity limit of the analysis

3.1.2 Fit to the data

For each Higgs boson mass hypothesis, three successive fits were performed :

- First a Gaussian + constant fit was applied on the signal simulation, in a mass window of total width 4 GeV/c^2 centered at the generated mass. This fit will be further referred to as "signal".
- Then a fourth order polynomial was fitted to the data in a large window, inside of which the previous 4 GeV/c^2 was excluded. This fit will be further referred to as "data".
- Finally a global fit ("data" + $\alpha\times$ "signal") was done on the data either
  - in a large window allowing the parameters of the polynomial and the parameter α to vary (six parameter fit),
  - or in the 4 GeV window, using a two parameter (α and β) fit, with β being a normalization coefficient for "data".

Both fits gave similar results, for α and its error.

Numbers obtained for four different masses are displayed in Table 3. Similar fits were performed for all mass hypotheses from 28 to 43 GeV/c^2 in 1 GeV steps, using for "signal" interpolated values of the four parameters. From these fits the 95% confidence level for the maximum value of α compatible with the data was deduced and from this the limit (at the 95% confidence level) of sensitivity is drawn on Figure 8 (curve b). Three conclusions could be drawn :

- in the region 28 to 38 GeV/c^2, α is small and positive, and its upper limit is well below 30%.
- in the region 38 to 43 Gev/c^2, α is found negative, which is a strong argument for a very low limit of sensitivity. When the fit was performed with a bounded parameter, α remained at its bound (zero) with a very small error.
- above 43 Gev/c^2, the method could not be applied because there were too few bins on the right hand side of the expected signal to get a stable result for the fit through the data.

3.1.3 Conclusion for the hadronic channel

From Figure 8, it is clear that the second method, which do not rely on a simulation of the background, gives roughly similar results to the first one, in the range of masses where it is applicable. The first method was found to be less sensitive than the second in the high mass region, but the second method fails to give a result above 43 GeV/c^2. The limit of sensitivity had been chosen as the one from the first method (curve a) for the low mass region (below 35.5 GeV/c^2) and above 43 GeV/c^2 while the other method was used for the intermediate mass region. Thus, a 95 % confidence level (CL) lower limit for the mass of a charged Higgs particle decaying hadronically was determined to be 43.5 GeV/c^2, and from the ratio of the sensitivity limit to the number of expected signal events a domain was excluded in the plane (Higgs boson mass vs. Br(Higgs $\rightarrow$ hadrons)) as shown on Figure 9, curve a.

3.2 Leptonic channel

If the branching fraction for the decay channel $H^+ \rightarrow \tau^+\nu_\tau$ is high, it is possible to search for events in which both charged Higgs particles decay leptonically. In this case the final state will consist of an acoplanar pair of low multiplicity jets coming from the decay of the τ's. DELPHI has already reported the results of a search for this type of event in the previous publication on charged Higgs particle search [3], which has been updated in the context of a search for sleptons and charginos [11]; here the points of the analysis which are more relevant for the H^+H^- channel will be recalled.

The search was based on approximately 330,000 Z^0 decays collected in 1990 and 1991. The selection criteria required that the event could be clustered into two jets, each with masses below 2 GeV/c^2 and 1 to 3 charged particles, but with no more than 4 particles in total. The two jets were required to have a momentum greater than 3 GeV/c each and the acoplanarity angle between them was required to exceed 16°. Events where there was a photon at more than 15° from both jets were rejected, as were those in which the component transverse to the beam axis of the total momentum of the charged particles was lower than 3.5 GeV/c. Four events survived the selection. However, they all

had two identified leptons of the same flavour (three ee and one $\mu\mu$) as expected from photon-photon interactions, which constitute the main background process. Rejecting such combinations reduces the $\tau^+\tau^-\nu\nu$ signal by a factor of 0.92 . The total selection efficiency for a pair of charged Higgs bosons with a mass around 45 GeV/c^2 was calculated to be 31%, including reconstruction losses. Since there were no candidate events, this excluded at 95% confidence level a charged Higgs boson with a mass lower than 45.4 GeV/c^2 for Br($H^+ \to \tau^+\nu_\tau$) = 1, as well as the domain limited by curve b on Figure 9.

3.3 Global mass limit

Combining results from sections 3.1 and 3.2, a new global mass limit in the plane $m_{H^\pm}$ vs Br($H^\pm \to$ hadrons) can be deduced and is plotted in Figure 9. Taking into account the previously excluded mass range, the new lower limit on the mass of a charged Higgs boson, at the 95% confidence level, is 43.5 GeV/c^2, independent of its decay branching fraction into hadrons.

4 Inference for other pair-produced scalars

4.1 Neutral Higgs particles in a two doublet scheme

Since the jet-jet mass resolution is similar for the $c\overline{c}$, $b\overline{b}$ and $c\overline{s}$ systems, the same 4-jet analysis allows a complementary search for the neutral Higgs bosons via Z$\to$ hA $\to c\overline{c}c\overline{c}$ (the dominant decay when $\tan\beta \ll 1$), Z$\to$ hA $\to c\overline{c}b\overline{b}$ or Z$\to$ hA $\to b\overline{b}b\overline{b}$ under the restrictive condition that h and A have the same mass. In this case, the general formula of the production of a hA pair can be simplified to :

$$\Gamma(\mathrm{Z} \to \mathrm{hA}) \approx 0.5\ (1 - 4\mathrm{m}_\mathrm{h}^2/\mathrm{m}_\mathrm{Z}^2)^{3/2}\Gamma(\mathrm{Z} \to \nu\bar{\nu})\cos^2(\alpha - \beta) \quad (\text{when } \mathrm{m_h} = \mathrm{m_A})$$

The results from Table 3 can thus be translated into limits on $\cos^2(\alpha - \beta)$. Since limits on $\sin^2(\alpha - \beta)$ can be derived from the Standard Model Higgs boson analysis [12], a given m_h can be excluded provided the sum of the limits falls below 1. This sum was estimated to be .76 $\pm$.02 for m_h = 44 GeV/c^2 and 1.01 $\pm$.03 for m_h = 44.5 GeV/c^2. Thus a 44.4 GeV/c^2 neutral Higgs boson can be excluded at the 95% confidence level. This result also applies when m_h is not strictly equal to m_A because the constrained fitting procedure only begins to degrade when the mass difference exceeds 4 GeV/c^2.

4.2 Diquarks

Diquarks appear in several theoretical approaches and models extending the Standard Model; recently [13] they appear in E_6 inspired superstring theory as members of new supermultiplets of E_6, which has been considered as an attractive basis for grand unification for a long time. In this formulation, each matter generation lies in a $\underline{27}$ representation and in addition to the light fermions of the SM and their SUSY partners, extra colour-triplet spin 0 and spin 1/2 particles, D, are predicted for each family. There are two spin 0 new particles, D_0 and D_0^c, their charge being $-1/3$ and they could behave as either pure elementary leptoquarks (L= +1, B= +1/3) or pure elementary diquarks (L= 0, B= $-2/3$). If the D particles behave as diquarks, then the dominant decay modes would be $D_0 \to \bar{q}\bar{q}'$, $D_0^c \to qq'$, and $D_{1/2} \to \bar{q}\bar{q}'\chi$, where χ is the lightest supersymmetric neutral

particle. These D_0 decays may only be detectable in the $e^+e^- \to D_0\bar{D}_0$ ($D_0^c\bar{D}_0^c$) channels [14].

The expected cross section in each family, including QED and electroweak corrections, is smaller than the H^+H^- one by a factor 2 if the two diquarks of the same family are mass degenerate and there is no mixing between them, otherwise it is smaller by a factor of 4.

The signature for pair production from the second family would be $e^+e^- \to D_0\bar{D}_0 \to \bar{c}\bar{s}cs$, which is similar to the one from a pair of charged Higgs particles decaying hadronically. Thus it is tempting to use the same analysis in a search for this process. However, diquarks are coloured objects and coloured strings develop in a different way from the case of a colorless Higgs boson pair. The effects of these different fragmentation schemes were studied in detail by comparing samples of generated $D_0\bar{D}_0$ and H^+H^- events at masses in the range 20-40 GeV/c^2 and fitting the distributions of the di-jet masses obtained after the 4-jet global constrained fit described in section 2.1. The observed results were a broadening of the width and a shift of the di-jet mass for the $D_0\bar{D}_0$ events relative to the H^+H^- case. The broadening of the width decreased from 25% at 20 GeV/c^2 to 12% at 40 GeV/c^2 and the shift of the mass decreased from 12% at 20 GeV/c^2 to 0.5% at 40 GeV/c^2.

The same test as that of Table 3 (section 3.1.2) was applied, and the corresponding result is shown in Figure 10. The poorer sensitivity limit is due to the broadening of the width mentioned above and affects mainly the region below 37 GeV/c^2. From that figure, diquarks can be excluded at the 95% confidence level from 28 to 43 GeV/c^2 if they are mass degenerate, and from 28 to 31.7 GeV/c^2 otherwise.

For lower diquark masses, a dedicated analysis [15] was performed using 387,000 hadronic Z^0 events (1990 + 1991 data), 231,000 hadronic simulated events and the existing "signal" of simulated H^+H^- events with masses 15-37 GeV/c^2. The same global 4-jet constrained fit was applied and the same quality selection criteria were used (section 2.1). The di-jet mass distribution of the H^+H^- samples were smeared to take into account the broadening effect due to the different fragmentation scheme of the diquark pair.

Instead of the F cut which was best adapted for higher masses, a set of kinematical cuts optimized for each of the various signal masses was applied, drastically reducing the QCD background. These included the energy difference between the fastest and the slowest jets, the sum of the decay angles of the two heavy objects, sphericity, etc. No signal was seen in the mass range 15-35 GeV/c^2, as shown on Figure 11, thus excluding pair production of mass-degenerate diquarks of the second family in this same mass interval at the 95% confidence level, and of non-degenerate diquarks up to 28 GeV/c^2. Thus, combining this result with the result above, and taking into account the fact that this analysis does not distinguish the jet flavors, a diquark of the E_6 type can be excluded in the interval 15 - 43 GeV/c^2 at the 95% confidence level (mass degenerate without mixing) and in the interval 15 - 31.7 otherwise.

5 Conclusion

Based on an analysis of 1.7 million hadronic Z^0 decays, new lower limits have been set on the mass of possible heavy pair-produced scalar-particles. All these limits should be understood as 95% confidence level limits.

- For the charged Higgs boson, the limits are

$$\begin{aligned} m_{H^\pm} &> 43.5 \text{ GeV}/c^2 \qquad \text{for } Br(H^+ \to c\bar{s}) = 1 \\ \text{and } m_{H^\pm} &> 45.4 \text{ GeV}/c^2 \qquad \text{for } Br(H^+ \to \tau^+\nu_\tau) = 1 \end{aligned}$$

  leading to a combined limit of 43.5 GeV/c^2, irrespective of the Higgs boson decay branching ratios.
- For the neutral Higgs bosons in a two doublet model, the lower mass limit is

$$m_h > 44.4 \text{ GeV}/c^2 \qquad \text{for } m_h \simeq m_A$$

- E_6 diquarks have been excluded in the mass range 15 - 31.7 GeV/c^2, this range being extended up to 43 GeV/c^2 if these diquarks are degenerate in mass.

It should be noted that the present results set mass limits essentially at the LEP I kinematic limits.

Acknowledgements

We are greatly indebted to our technical collaborators and to the funding agencies for their support in building and operating the DELPHI detector, and to the members of the CERN-SL Division for the excellent performance of the LEP collider.

References

[1] P. J. Franzini *et al.*, Z^0 physics at LEP1, Higgs search, CERN 89-08, vol.2, p.59.

[2] JADE Collaboration, W. Bartel et al., *Phys. Lett.* **114B**(1982)211
TASSO Collaboration, M. Althoff et al., *Phys. Lett.* **122B**(1983)95
CELLO Collaboration, H.J. Behrend et al., *Phys. Lett.* **193B**(1987)376

[3] DELPHI Collaboration, P. Abreu et al., *Phys. Lett.* **241B**(1990)449

[4] ALEPH Collaboration, D. Decamp et al., *Phys. Reports* **216**(1992)254
L3 Collaboration, O. Adriani et al., *Phys. Reports* **236**(1993)1
OPAL Collaboration, M.Z. Akrawy et al., *Phys. Lett.* **242B**(1990)299

[5] T. Sjöstrand, Comp. Phys. Comm. **28** (1983) 227
T. Sjöstrand and M. Bengtsson, Comp. Phys. Comm. **43** (1987) 367.

[6] DELPHI Collaboration, P. Aarnio et al., *N.I.M.* **A303**(1991) 233

[7] JADE Collaboration, W. Bartel et al., *Zeit. Phys.* **C33** (1986) 23.

[8] G. C. Fox and S. Wolfram, *Phys. Lett.* **82B** (1979) p.134.

[9] N. J. Kjær, Ph.D. thesis, Niels Bohr Institutet Kopenhagen, 1991

[10] R. A. Fisher, *Annals of Eugenics*, vol.7 (1936).

[11] DELPHI Collaboration, P. Abreu et al., *Phys. Lett.* **B247**(1990)157
A. Lopez-Fernandez, Proceedings of the 1992 Fermilab Meeting, Vol. 2 p. 1221; World Scientific 1993.

[12] DELPHI Collaboration, P. Abreu et al., CERN-PPE / 94-46 /Rev, to be published in Nucl. Phys. B.

[13] D. Schaile and P. Zerwas in Proc. Workshop on Physics at future accelerators (La Thuile and Geneva) CERN Report 87-07 Vol II p.251.
J. Ellis and F. Pauss, ibid. Vol I p.80.

[14] V. D. Angelopoulos *et al.*, *Nucl. Phys.* **B292** (1987) 59

[15] E. Katsoufis, A Search for Elementary Scalar Diquarks, DELPHI note 92-126 PHYS 226.

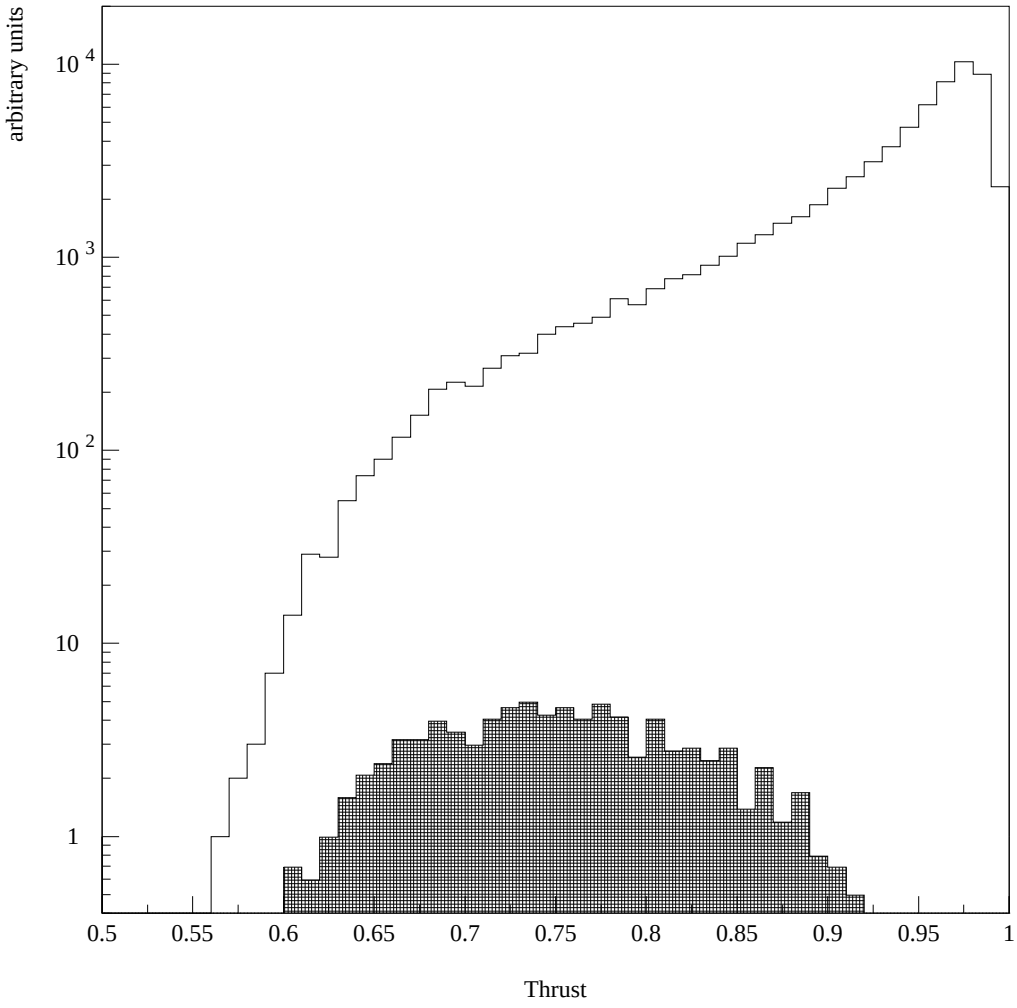

Figure 1: Distribution of Thrust for H^+H^- events (grey) for a Higgs particle mass of 40 GeV/c^2 and real data $Z^0 \rightarrow$ hadrons (plain). Note the vertical log scale.

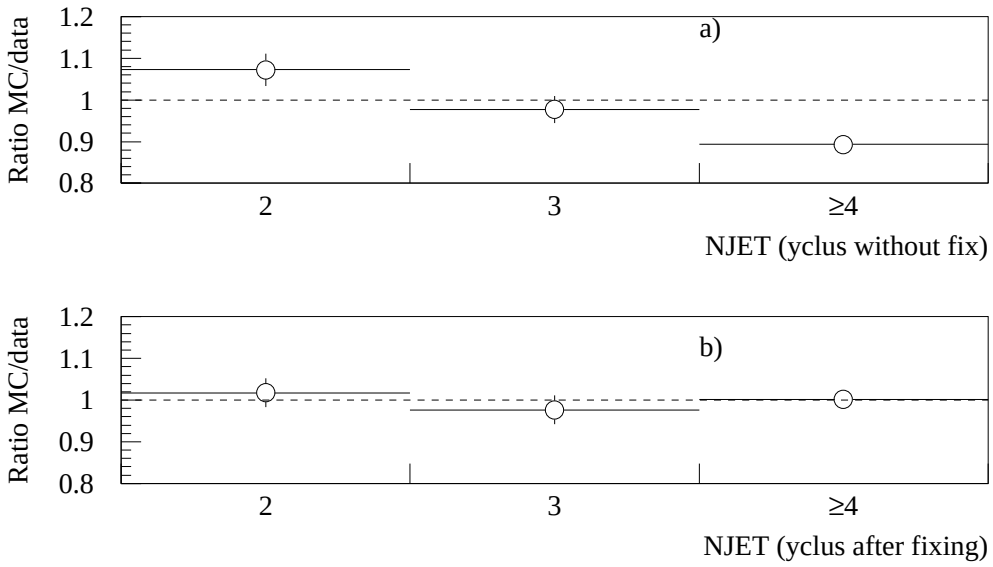

Figure 2: MC/data ratio versus NJET found with YCLUS. The top figure is before fixing, the bottom one is after fixing as described in the text.

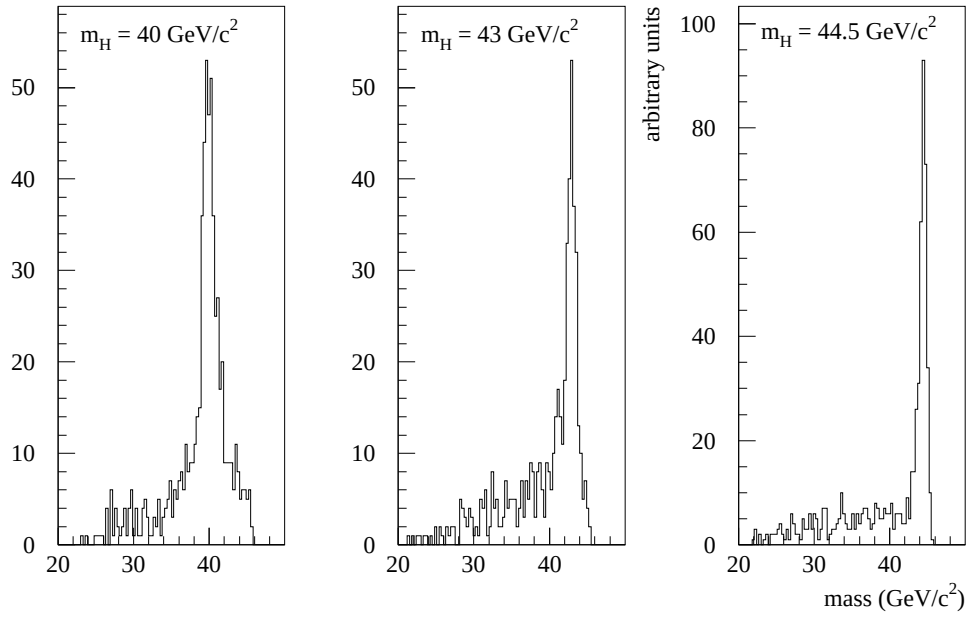

Figure 3: Mass distributions obtained after constrained fitting of simulated events for three Higgs boson masses. Full widths at half maximum are respectively 1.7 (1.1) (0.8) GeV/c^2 at m_H = 40 (43) (44.5) GeV/c^2.

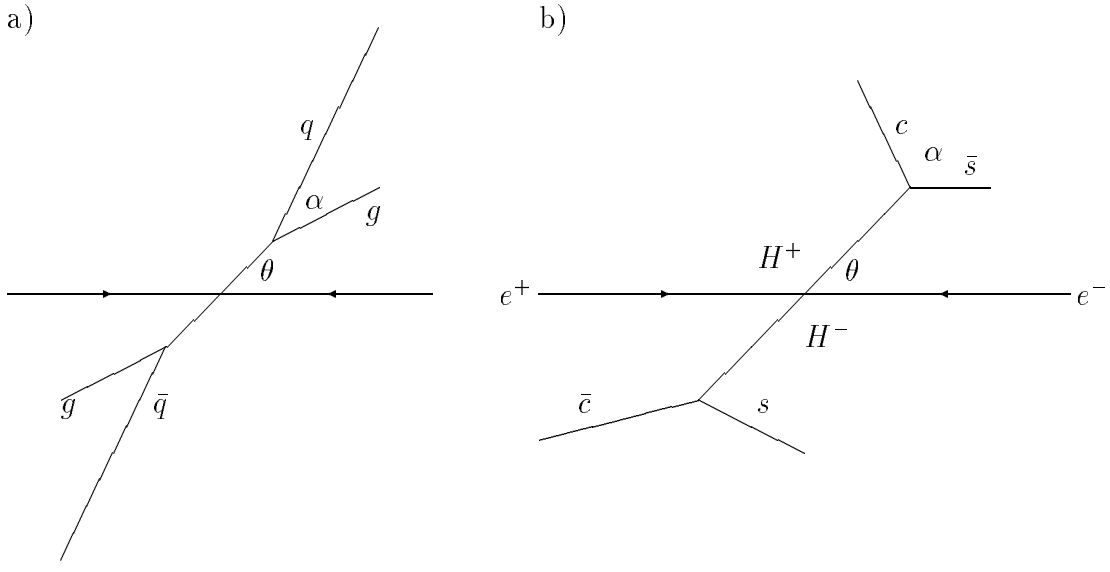

Figure 4: Schematic diagrams of a) background, b) signal events.

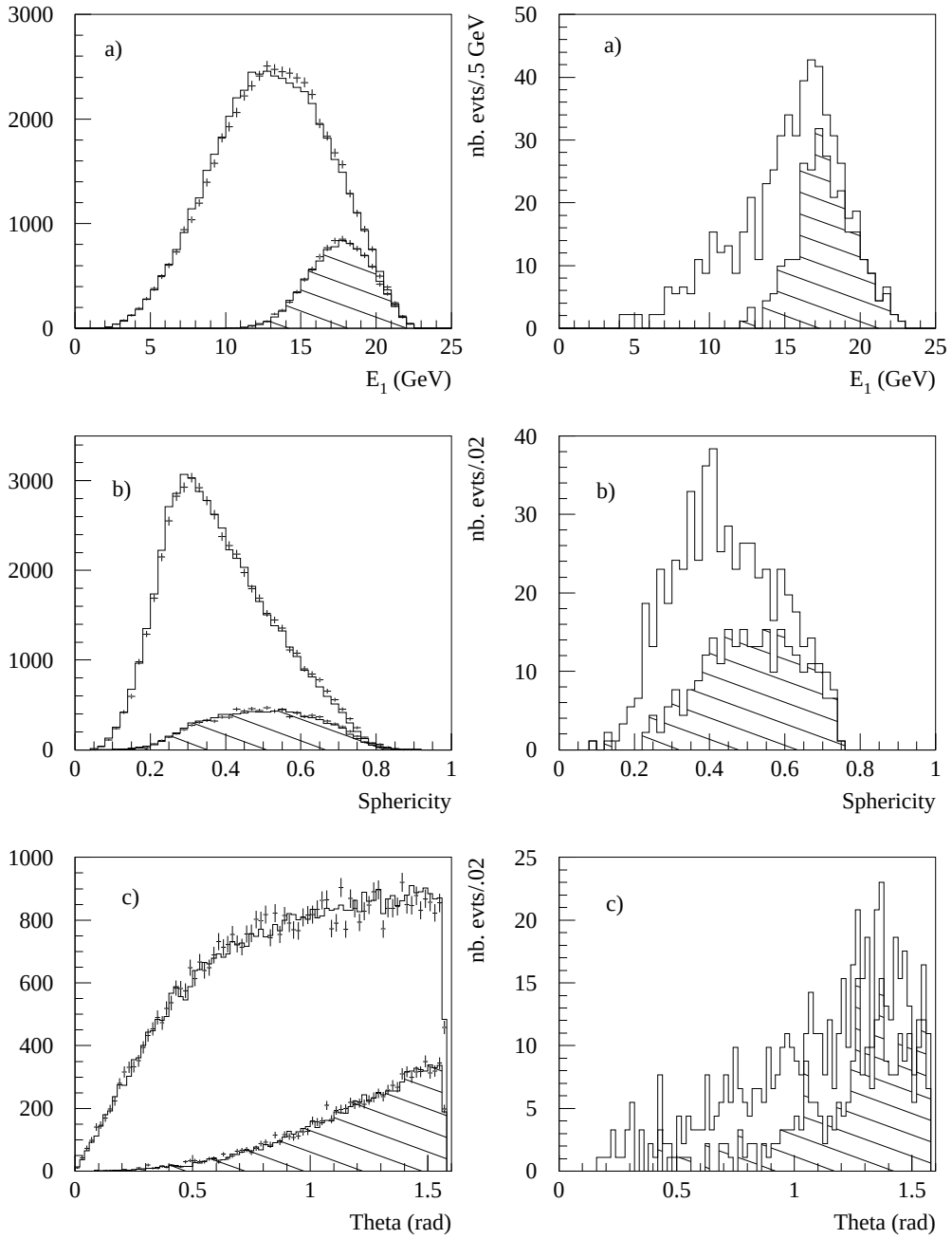

Figure 5: On the left side, distributions of a) E_1 (energy of the least energetic jet), b) sphericity and c) θ ($H^{\pm}$ polar production angle) for data (crosses) and simulation (histograms). On the right side, the same distributions in the case of the hadronic decay of charged Higgs boson pairs (43 GeV/c^2). Events passing the multi-dimensional cut (equ. (2)) are shaded.

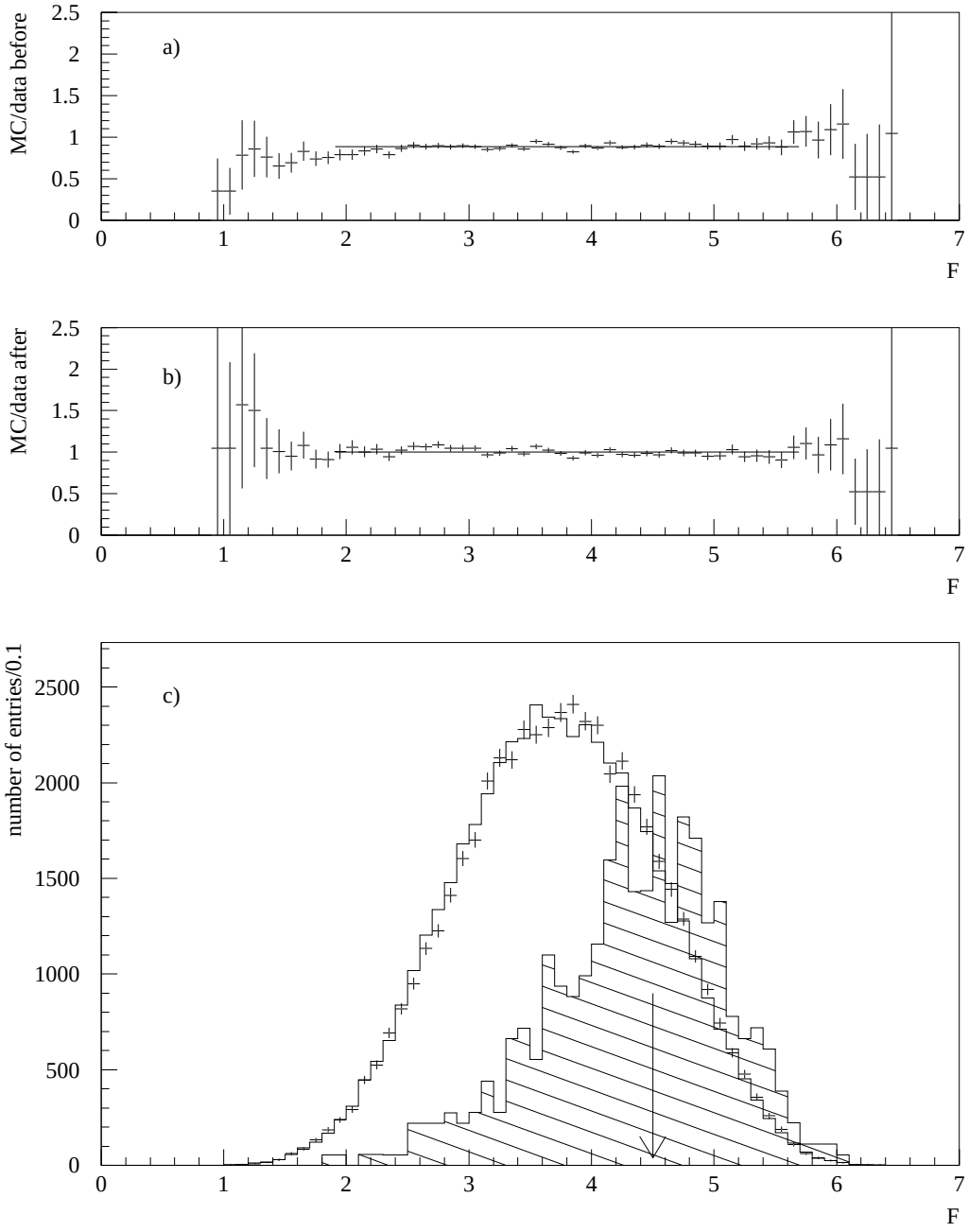

Figure 6: Above, MC/data ratio as a function of F (see equation (2) for definition), a) before and b) after y_{cut} fixing. The fits of this ratio to a constant value give the following results : a) 0.885 and $\chi^2 = 44.3$ for 37 degrees of freedom and b) 0.999 and $\chi^2 = 43.2$ for the same number of degrees of freedom. Below (c), distribution of the variable F for $q\overline{q}$ simulation (histogram), DELPHI data (crosses) and for a 43 GeV/c^2 charged Higgs boson (hatched histogram, not to scale). The cut at 4.5 is indicated by the vertical arrow.

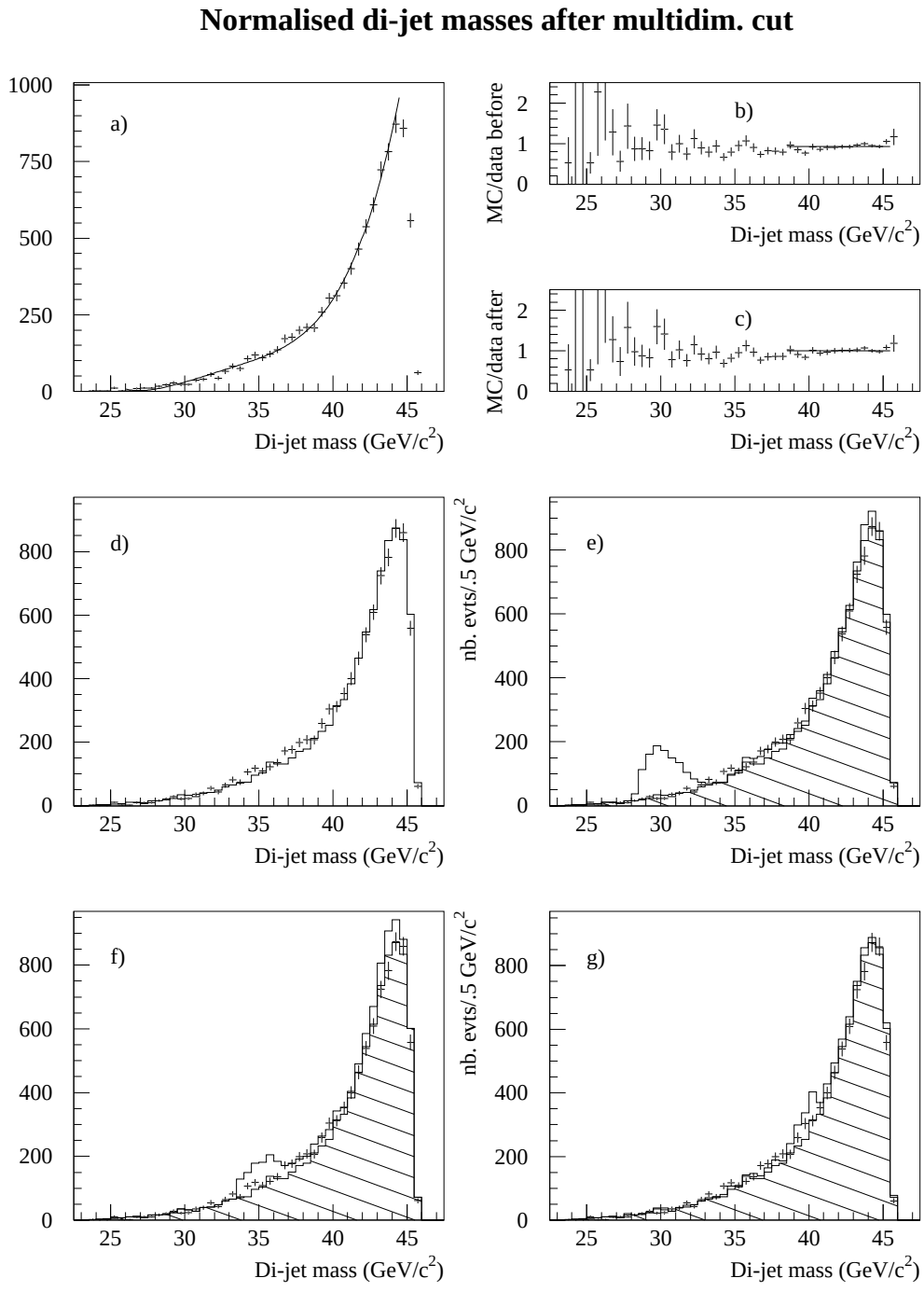

Figure 7: a) Di-jet mass spectrum for DELPHI data (crosses) and result of a polynomial fit. b) and c) MC/data ratio as a function of the di-jet mass, respectively before and after y_{cut} fixing. The fit results are : b) 0.925 and $\chi^2 = 15.7$ for 12 degrees of freedom, c) 0.996 and $\chi^2 = 11.5$ for 12 degrees of freedom. d) Comparison between di-jet mass spectra for simulation (histogram) and data (crosses), reproduced also on the three last plots. In the last three pictures, the unshaded areas are the expected signals for different Higgs boson masses : e) 30 GeV/c^2, f) 35 GeV/c^2, g) 40 GeV/c^2.

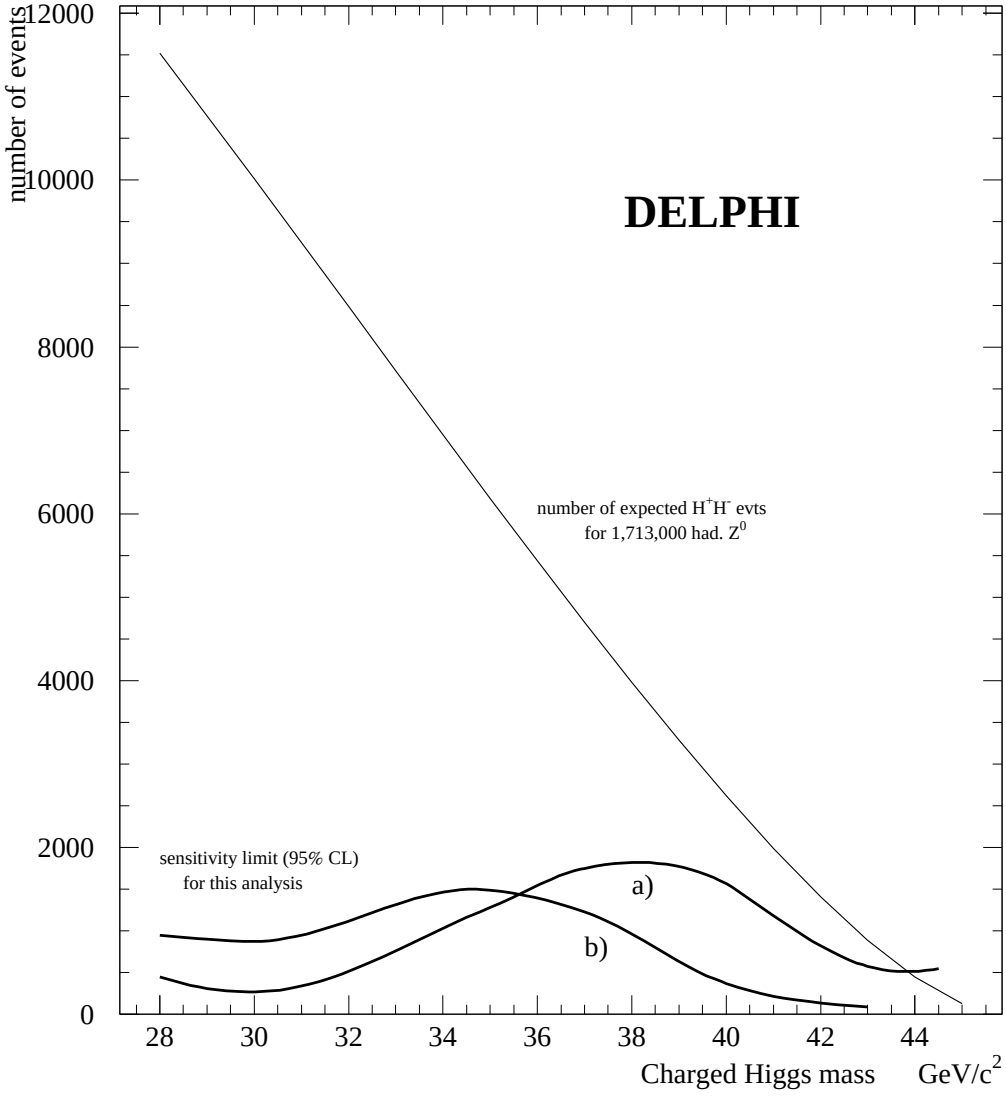

Figure 8: Limit of sensitivity of the hadronic analysis (two methods), compared with the total number of expected signal events, showing clearly the exclusion interval from 28 to 43.5 GeV/c^2. Curve a) is obtained by a direct comparison of data versus background and curve b) by a fit to data + $\alpha\times$ signal.

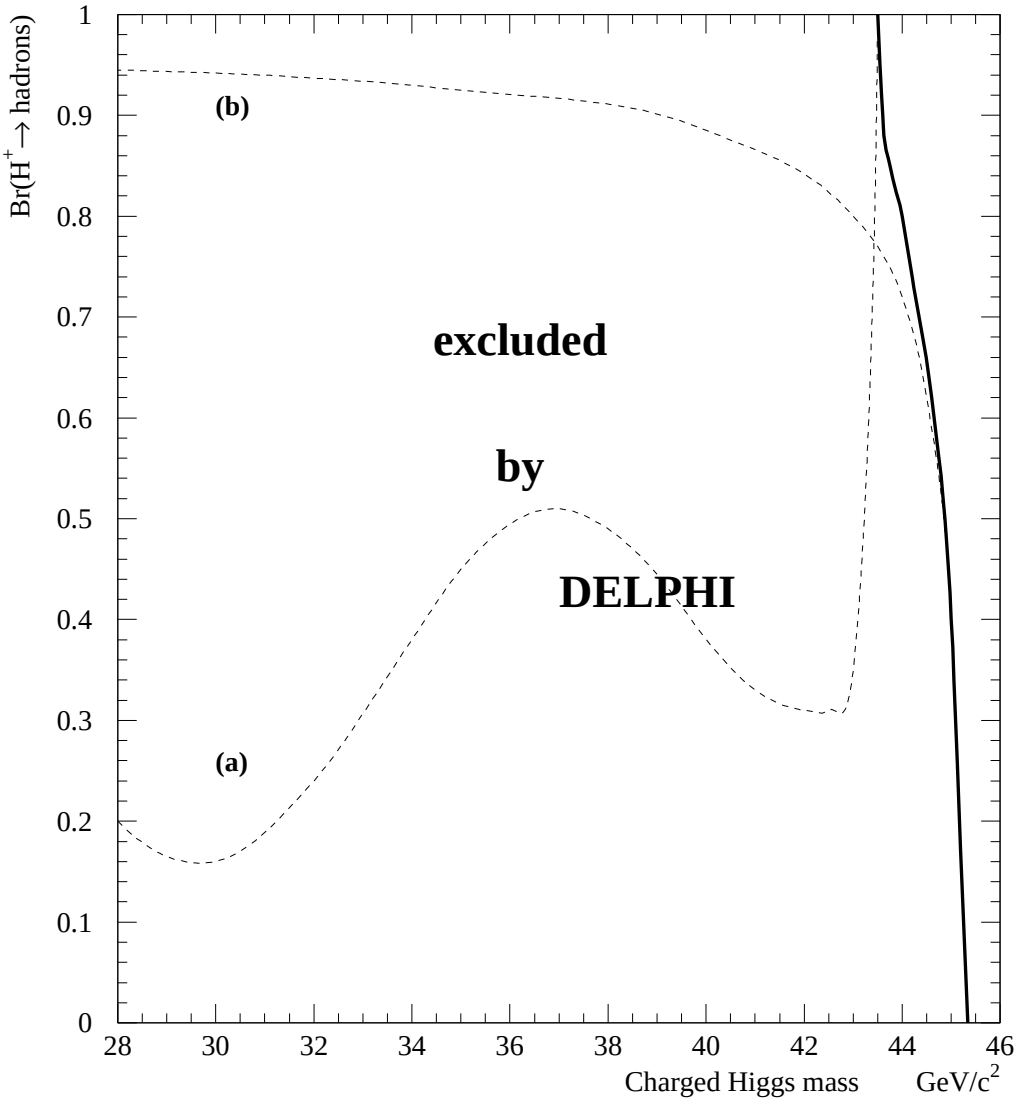

Figure 9: Excluded regions at 95% confidence in the plane $m_{H^\pm}$ vs $Br(H^\pm \to \text{hadrons})$. The region above curve (a) is excluded by the hadronic analysis, while the region below curve (b) is excluded by the $\tau\tau$ analysis. The bold solid curve on the right hand side corresponds to the combined limit.

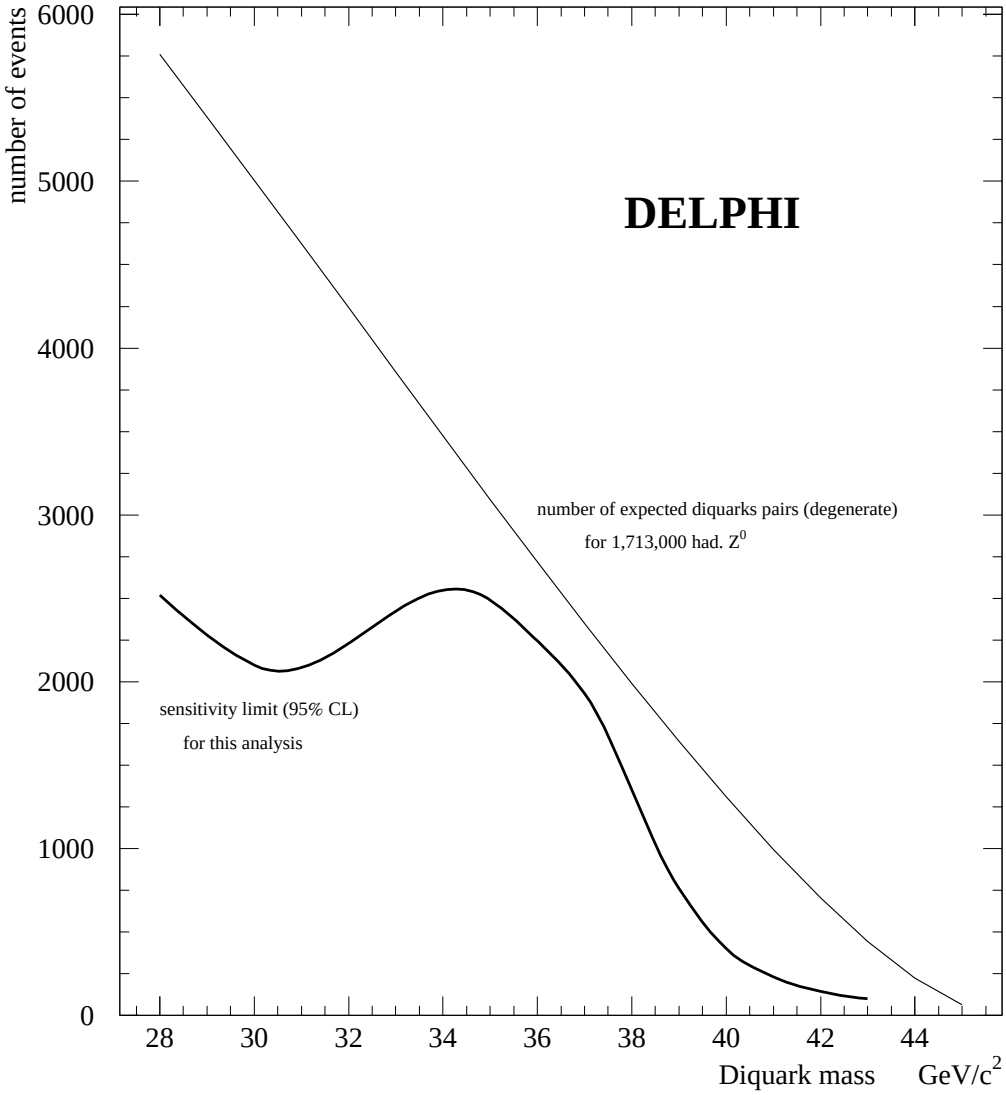

Figure 10: Limit of sensitivity of the diquark analysis, compared with the total number of expected signal events, showing clearly the exclusion interval from 28 to 43 GeV/c^2.

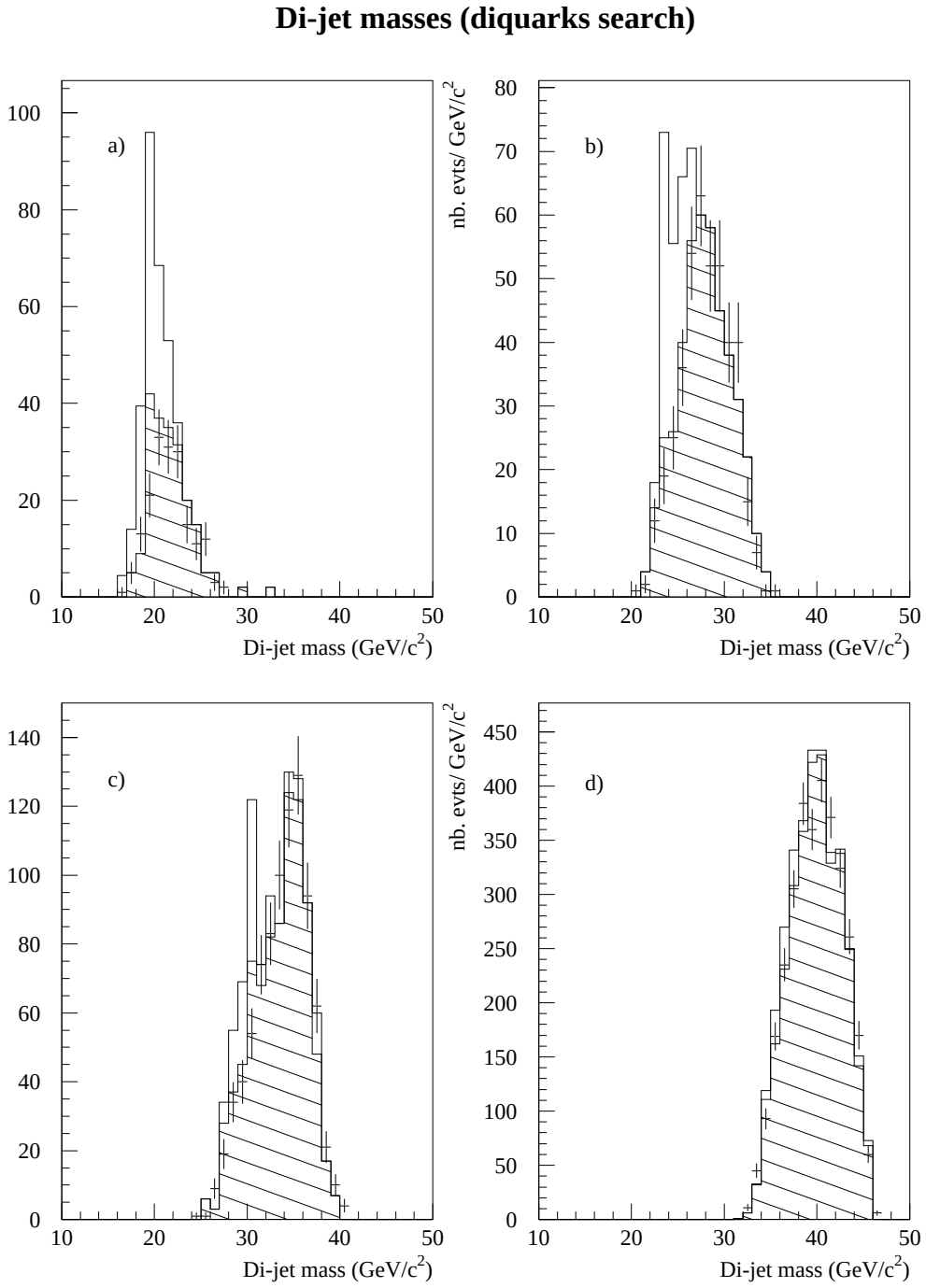

Figure 11: Comparison between di-jet mass spectra for simulation (shaded histogram) and data (crosses), together with the expected diquark signals (unshaded) for different diquark masses : a) 17.5 GeV/c^2 non-degenerate, b) 23 GeV/c^2 non-degenerate, c) 29 GeV/c^2 degenerate and d) 36.5 GeV/c^2 degenerate diquarks.